# The INES System IV: The IUE Absolute Flux Scale

R. González-Riestra<sup>1,\*</sup>, A. Cassatella<sup>2,3,\*</sup>, and W. Wamsteker<sup>4,\*\*</sup>

- <sup>1</sup> Laboratorio de Astrofísica Espacial y Física Fundamental, VILSPA, P.O. Box 50727, 28080 Madrid, Spain
- <sup>2</sup> Istituto di Astrofisica Spaziale, CNR, Area di Ricerca Tor Vergata, Via del Fosso del Cavaliere 100, 00133 Roma, Italy
- <sup>3</sup> Dipartimento di Fisica E. Amaldi, Universitá degli Studi Roma Tre, Via della Vasca Navale 84, 00146 Roma, Italy
- <sup>4</sup> ESA-IUE Observatory, VILSPA, P.O. Box 50727, 28080 Madrid, Spain

Accepted: May 4, 2001

**Abstract.** This paper deals with the definition of the input fluxes used for the calibration of the IUE Final Archive. The method adopted consists on the determination of the *shape* of the detector's sensitivity curves using IUE low resolution observations with model fluxes of the DA white dwarf G191–B2B. A *scale factor* was then determined so that the IUE observations of some bright OAO–2 standards match the original measurements from Meade (1978) in the spectral region 2100–2300 Å. The ultraviolet fluxes of six standard stars used as input for the Final Archive photometric calibration together with the model fluxes of G191–B2B normalized to the OAO–2 scale are given. A comparison with the independent FOS calibration, shows that the IUE flux scale for the Ultraviolet is 7.2 % lower. We consider this mainly to be caused by the different normalization procedures. It is shown that the present flux calibration applies to spectra processed with the *INES* low resolution extraction software.

**Key words.** Methods: data analysis – Space vehicles: instruments – Astronomical databases: miscellaneous – Ultraviolet: general

#### 1. Introduction

Many improvements have been made to the standard processing of IUE data along the years. The combination of a better understanding of the instruments and the rapid evolution of computing capabilities, has allowed to use the carefully planned calibration data, obtained under well controlled acquisition conditions over the 18 years of the IUE Project, to prepare a new calibration of the complete IUE data set.

The IUE Final Archive, *IUEFA*, was the end-product of the above process, which started to be defined in the late eighties. The processing software developed for this purpose was *NEWSIPS* (Garhart et al. 1997). The *INES* (IUE Newly Extracted Spectra) System is the final configuration of the IUE archive.

A detailed revision of the *NEWSIPS* output products indicated that there were still some problems which could be corrected. The most important deficiency was found in the *NEWSIPS* extraction and noise models for low resolution spectra (*SWET*), which e.g. caused emission line

Send offprint requests to: R. González-Riestra, e-mail: ch@laeff.esa.es

fluxes to be frequently wrongly extracted (Schartel and Skillen, 1998). In high resolution data, a systematic mismatch of about 20 km s<sup>-1</sup> between the velocity scales of short and long wavelength spectra was present. These, together with other errors, were corrected in the *INES* system developed by the ESA IUE Observatory (Wamsteker et al. 2000). A full description of the *INES* system and its data processing is given in Rodríguez-Pascual et al. (1999), Cassatella et al. (2000) and González-Riestra et al. (2000). The *INES* Data are available from the *INES* Principal Centre http://ines.vilspa.esa.es or from the *INES* National Hosts (Wamsteker 2000). For details on the instrumental history of IUE see Pérez-Calpena and Pepoy (1997).

In this paper we discuss the way the IUE absolute flux scale was redefined (Sect. 2 and 3). The specific algorithms needed to optimize the internal consistency of IUE spectra, such as those used to determine the effective exposure times and to correct for the time and temperature dependency of the sensitivity of the IUE cameras are described in Sec. 3. In Sec. 4.2, a comparison is made between fluxes obtained through the present calibration and those derived from previous IUE calibrations and from other experiments (HST and HUT). In Sec. 4.3 we demonstrated

<sup>\*</sup> Previously: ESA-IUE Observatory

<sup>\*\*</sup> Affiliated to the Astrophysics Division, SSD, ESTEC

strate the applicability of the our calibration to the data in the *INES* archive.

#### 2. The IUE Flux Scale

Along the operational life of IUE, and prior to the Final Archive processing, several photometric calibrations algorithms have been applied as a consequence of the changes made in the processing software. In all cases the flux calibration was based on the UV absolute fluxes of the bright B3 V standard star  $\eta$  UMa (V=1.84) as defined by Bohlin et al. (1980). However, evidence for systematic errors in this  $\eta$  UMa flux scale made it necessary to find alternatives to be used as primary calibration standards for the IUE Final Archive. In this Section we will describe the basis of the early IUE photometric calibrations and the new flux scale.

The primary flux calibration for IUE data is done on the low resolution spectra, while the high resolution calibration is derived from this. The common basis of all early calibrations was the absolute flux of  $\eta$  UMa defined by Bohlin et al. (1980), who took the OAO-2 data as main reference for fluxes longward 2000 Å, and the rocket data of Brune et al. (1979) for shorter wavelengths.  $\eta$  UMa is too bright to be observed directly with IUE at low dispersion, and therefore a set of secondary standard stars was defined. These were chosen from the OAO-2 and TD1 Catalogues. The original OAO-2 and TD1 fluxes of these standards were reduced to the common  $\eta$  UMa flux scale by applying the "correction factors" given by Bohlin and Holm (1984).

With the growing observational material acquired over the years, it became clear that there were systematic differences between observations and models for objects of very different physical nature, such as white dwarfs (Greenstein and Oke 1979), BL Lac objects and sdO stars (Hackney et al. 1982). Finley et al. (1990) showed discrepancies of up to a 15% when comparing IUE observations and fluxes predicted by models of DA white dwarfs. The fact that these differences were maximum in the region of largest disagreement between the original OAO–2 and TD1 fluxes, pointed to the existence of systematic errors in the  $\eta$  UMa flux scale.

A complete revision of the IUE flux calibration was therefore considered a primary requirement in the planning of the IUE Final Archive (Cassatella 1990). Rather than deriving the flux scale for the UV on a star which can not be observed with the instrumental setup supplying the bulk of currently available UV data, a different approach was taken, allowing to use the IUE large data set and to make new special purpose observations to derive an independent calibration. Hot DA white dwarfs were chosen as the most suitable objects to define the relative IUE flux scale. They were used to determine the shape of sensitivity curves by comparison of the IUE observations with model fluxes. A scaling factor was defined to bring the relative fluxes of the OAO-2 standards at an absolute scale. In the absence of other (and better) calibration sources for the

Table 1.

Number of spectra used to derive the Absolute Fluxes of the Standard Stars

Wavelength	G191-B2B	Bright	Faint	
Range		$Stars^1$	$Stars^2$	Total
Short	19	39	45	103
Long	19	43	66	128

Number of spectra used to derive the Inverse Sensitivity Curves of the IUE Cameras

	Bright	Faint	
Camera	$Stars^1$	$Stars^2$	Total
SWP	29	104	135
LWP	14	91	105
LWR	22	41	63

 $<sup>^{1}</sup>$   $\eta$  Aur,  $\lambda$  Lep, 10 Lac,  $\zeta$  Dra

space—UV, the absolute scale was defined by the original OAO-2 measurements from Meade (1978). The accuracy on computed fluxes for DA white dwarfs is discussed by Finley (1993).

To obtain the shape and the scale factor of the sensitivity curves, an intensive observing campaign was made in 1990 and 1991. These observations included not only the traditional TD1 and OAO–2 standards already in use, but also a selected sample of DA white dwarfs. Details of the procedure followed to obtain the input fluxes for the IUE calibration are given in the next Section.

#### 3. The calibration of the IUE Final Archive

#### 3.1. The input Data

Two sets of data were used to derive the flux calibration for the IUE Final Archive. The first one consisted of a large number of observations of the IUE standard stars taken at the time of the acquisition of the 1984–85 Intensity Transfer Functions (hereafter ITFs). This set included spectra obtained in all the possible observing modes (high and low dispersion, large and small aperture, trailed, etc).

A considerably more extended set of calibration data was taken is 1991, which included not only observations of the IUE standard stars, but also of several selected white dwarfs, and in particular G191–B2B. The acquisition of these data was carefully planned to determine all parameters necessary for the calibration of the instruments, such as the size of the spectrograph apertures and the camera response times. The 1991 data were used to derive the absolute fluxes of the IUE standard stars. The use of close—in—time observations of both the white dwarfs and the standard stars avoided the need to correct for the cameras sensitivity loss.

Only point–source Large Aperture spectra were used for the derivation of the flux calibration. As part of

<sup>&</sup>lt;sup>2</sup> BD+28 4211, BD+75 325, HD 60753

the complete calibration of the IUE instrument, the factors necessary to calibrate other observational modes, e.g. trailed spectra, were redetermined.

Table 1 gives the number of standard star spectra used to derive the photometric calibration of the IUE cameras.

# 3.2. The Intensity Transfer Functions (ITFs)

The ITFs are used to linearize the IUE raw Data Numbers (DNs) by transforming them into Flux Number (FNs). The ITFs are constructed from graded exposures of lamps under well controlled thermal spacecraft conditions and radiation background. For historical reasons these ITFs have been derived through linear interpolation between 12 selected exposure levels spaced over the dynamic range of the IUE Cameras (from 0 to 255 DN). This has made that some small linearity errors for the highest and lowest exposure levels have persisted in the IUE data (González–Riestra 1998). Since the ITFs define the linearity of the cameras, any calibration is linked to a specific ITF.

In what follows, we describe the ITFs used for the derivation of the IUE Final Archive flux calibration.

LWP: The original ITF for this camera was based on data obtained in 1984–1985. It was decided to acquire a new ITF in May 1992. Although some anomalies were found in the cross–correlation behavior of this ITF, its effects were limited and it was decided to maintain the 1992 ITF for the IUEFA processing. The existence of two well differentiated groups of zero level ("NULL") images, presented an additional anomaly. Although the cross–correlation behavior of one of these two (the "NULL-A") was worse, this was selected for the complete processing, since it avoided strong negative extrapolations at the short wavelength end of the camera.

LWR: The LWR camera was declared non-primary long wavelength camera in October 1983 (Pérez-Calpena and Pepoy 1997). A new ITF was acquired one month later. It was found that this ITF gave a poor correlation with science images, especially with those taken before the camera was declared non-operational. Two ITFs were constructed for this camera. ITF-A is the original 1983 ITF with its own NULL level. It is appropriate for most of the images taken after 1983. ITF-B has as NULL level the average of all the NULL images with similar geometric characteristics taken in the period 1978–1983. The upper levels are the same as in ITF-A, but resampled to match the geometric characteristics of this modified NULL level. The NEWSIPS processing cross-correlates every science image with both ITFs, choosing for the processing the one with the highest correlation coefficient. The use of two different ITFs in the photometric correction required to derive two inverse sensitivity curves for this camera.

 $\underline{\text{SWP}}\textsc{:}$  The ITF acquired in 1985 was used for the processing of all SWP images.

#### 3.3. The White Dwarf model

The white dwarf G191–B2B was selected as primary standard to define the relative fluxes of the other IUE standard stars due to its brightness (V=11.8), pure hydrogen atmosphere, high effective temperature (implying a narrow Lyman  $\alpha$  absorption line), and negligible interstellar absorption (N<sub>H</sub>  $\approx 1.7 \ 10^{18} \ {\rm cm}^{-2}$ , Kimble at al. 1993). The model used was provided by D. Finley (private communication, 1991), and was computed using the code of D. Koester (see a detailed description in Finley et al. 1997). The model has the following characteristics (see Fig. 2):

- Chemical composition: Pure Hydrogen
- $T_{\text{eff}} = 58000 \text{ K}$
- $-\log g = 7.5$

Evidence for the presence of metals in this star has been reported by Bruhweiler and Kondo (1981) and by Bruhweiler (1991) from IUE spectra, and by Vennes (1992) and Barstow et al. (1993) from ROSAT observations. However, the abundance of these elements is extremely low (C/H=2×10<sup>-6</sup>, N/H=4×10<sup>-6</sup>, Si/H=1×10<sup>-6</sup>, Fe/H=5×10<sup>-6</sup>, Ni/H=1×10<sup>-6</sup>; Wolff et al. 1998) and their influence in the IUE range is negligible. According to Finley (1993), the overlapping metal lines might reduce the FUV continuum by 1–2% in some spectral regions. The effective temperature and the gravity were derived from the profiles of the optical Balmer lines (Finley, private communication). The model provided by Finley was normalized to the spectrophotometric data in the range 3200–8000 Å as given by Massey et al. (1988).

The particular choice made here for the model parameters of G191–B2B, has a little effect on the IUE calibration in the sense that, if an improved model becomes available in the future, it would be straightforward to derive a suitable correction from the ratio between the new model and the one used here (see Appendix B).

#### 3.4. Other parameters and algorithms

## 3.4.1. Determination of exposure times

For very short exposures, the effective exposure time of the IUE cameras ( $t_{\rm eff}$ ) is different from the commanded one ( $t_{\rm com}$ ), due to the quantization of the clock (0.4096 sec.) and the so–called "Camera Rise/Fall time" (CRFT). New data were obtained to re–derive the rise/fall times in 1991 and the values used in the IUEFA production are given in Table 2 (González-Riestra 1991). The effective exposure time is:

$$t_{\rm eff} = INT(t_{\rm com}/0.4096) \times 0.4096 - t_{\rm rise}$$
 (1)

The actual duration of the shortest exposure times (less than 1 sec. for the brightest standard stars) is further affected by the Command Decoder Cycle Time (CDCT) which causes exposure times to be, 2/3 of the times 10.4 msec. longer than  $t_{\rm com}$ , and the remaining 1/3 is 19.6

Table 2. Camera Rise/Fall times

Camera	Rise time (sec)
LWP	$0.123 \pm 0.004$
LWR (at -4.5 kV)	$0.126 {\pm} 0.006$
SWP	$0.123 {\pm} 0.005$

**Table 3.** THDA dependence parameters

Camera	$T_{\rm ref}$	С
LWP	9.5	$-0.0046\pm0.0003$
LWR	14.5	$-0.0088 \pm 0.0004$
SWP	9.4	$-0.0019 \pm 0.0003$

msec. shorter (Oliversen 1987). This effect can be accounted for by taking a large number of spectra of the same star and comparing each individual observation with the average spectrum. The mean spectra of the bright standard stars used for the derivation of the calibration were obtained by averaging a sufficiently large number of spectra with identical exposure times and no correction for this effect in the individual exposure times was necessary.

# 3.4.2. Correction for temperature dependence

The sensitivity of the IUE cameras depends substantially on the temperature of the Camera Head Amplifier (THDA):

$$FN_{cor} = \frac{FN_{obs}}{1 + C \times (THDA - T_{ref})}$$
 (2)

where C represents the change in sensitivity introduced by a departure of one degree from the reference temperature,  $T_{ref}$ , (e.g. a difference of 5 degrees from  $T_{ref}$  represents a 2.5% sensitivity variation in the SWP camera). We have adopted the parameters given by Garhart (1991) to correct for this effect (Table 3).

# 3.4.3. The Time Sensitivity Degradation Correction algorithm

The zero epoch of the IUE calibration was defined to be 1985.0, because at this time the higher quality ITF observations were performed. This epoch was also taken as reference to correct for the loss of sensitivity of the IUE detectors. The procedure to derive the time sensitivity correction is fully described in Garhart et al. (1997). In short, fluxes in steps of 5 Å were derived for several hundreds of spectra of the standard stars covering the whole spacecraft lifetime and normalized to the average of spectra obtained near the reference epoch 1985.0. The ratios were binned into time steps of six months, and then fitted to polynomials over different time periods. For the LWP camera there are two approaches: after 1984.5, a linear fit is used. Before that epoch, there are few data available, and a linear interpolation between each pair of points is used. For

the LWR, a fourth order polynomial is used. For SWP, after 1979.5 a linear fit is used. Prior to this date the same approach as for the early LWP data is used. These corrections were all derived from pre–1990 data. The corrections were updated after the end of orbital operations to avoid the need for extrapolation.

As mentioned above, no correction for time—dependent sensitivity degradation was needed for the single epoch data used for the derivation of the flux calibration, and therefore no additional uncertainty was introduced in the calibration by the time dependent sensitivity correction algorithm.

#### 3.5. The Zero Point of the Absolute flux scale

The direct use of white dwarf atmospheres to define the absolute flux scale was discarded *a priori* by the IUE Project due to the possible errors implied in the determination of the stellar parameters. Normalization to optical photometry and/or spectrophotometry was also excluded to avoid the extrapolation over a wide spectral range, which could amplify substantially the errors.

We derived the zero point of the Final Archive absolute flux scale *directly* from *ultraviolet* observations. To this purpose we used as reference the OAO–2 fluxes in the 2100–2300 Å band. The reason for the selection of this window is that in this particular wavelength region the OAO–2 and the TD1 measurements show the best agreement (Beeckmans 1977).

The procedure used to obtain this scale factor was as follows:

- The 1991 calibration data were used to obtain average NET spectra (background–subtracted spectra in units of FN/s) in the LWP range for the four bright standard stars  $\eta$  Aur,  $\lambda$  Lep, 10 Lac and  $\zeta$  Dra for (all observed with OAO–2) and for G191–B2B.
- A preliminary LWP inverse sensitivity curve for 1991 data was obtained by dividing the above average LWP NET spectra of G191–B2B by the corresponding model fluxes (normalized to the optical spectrophotometry of Massey et al. 1998). A bi–cubic spline fit through the model fluxes has been used in this process.
- The NET 2100-2300 Å spectra of the four standard stars were first flux-calibrated using the preliminary inverse sensitivity curve and then compared with the average OAO-2 flux in the same band, as given in Meade (1978).

The result was that the OAO–2 fluxes of the four standards in the band 2100–2300 Å are on average lower by a factor of 1.042 than the ones obtained from IUE observations in the G191–B2B scale normalised to the optical spectrophotometry, as shown in Table 4.

Therefore, the model fluxes provided by Finley, after normalization to Massey et al. (1988) optical spectrophotometry, still had to be divided by a factor of 1.042 to agree with the OAO-2 absolute flux scale. This scal-

Table 4. The Zero Point Scale Factor

Star	G191–B2B scale/OAO–2 scale
$\eta$ Aur	$1.001 \pm 0.024$
$\lambda$ Lep	$1.025 \pm 0.029$
10  Lac	$1.062 \pm 0.024$
$\zeta$ Dra	$1.078 \pm 0.029$
Average	$1.042 \pm 0.035 \text{ (rms)}$

ing factor defines the UV absolute flux scale of the IUE instruments.

#### 3.6. The Inverse Sensitivity Curves

The procedure to derive the *relative* Inverse Sensitivity Curves (hereafter ISCs) of the SW and LW cameras in the low resolution mode was very similar. It can be summarized in two major steps:

- a) Determination of the absolute fluxes of the IUE standard stars from the 1991 data:
- Determination of a mean spectrum for each standard star from the 1991 observations (in units of Flux Number/sec).

All the spectra were individually inspected, rejecting those presenting any anomaly. All the exposure times were corrected for OBC quantization, THDA sensitivity and CRFT (see Section 3.4.1). The mean spectrum was computed by averaging all the available spectra and weighting each point by its associated error.

- Derivation of the 1991 ISC from the model and the mean spectrum of G191 B2B.
  - The WD model was divided by the mean spectrum, and the ISC was derived via a bi-cubic spline, excluding the region around Lyman  $\alpha$  and the spurious 1515 Å absorption (de la Peña 1992). The resulting curve was resampled in bins of 10 and 15 Å for the SW and LW cameras, respectively. Finally, the scaling factor of 1.042 (see above) was applied to the curves.
- Determination of the fluxes of the standard stars from the 1991 ISC.

The final ISCs were applied to the mean 1991 spectra of the standard stars in order to derive their absolute fluxes. The fluxes so obtained define the absolute flux scale of IUE data (see Appendix A).

#### b) Derivation of the ISCs for the 1985 Calibration epoch:

- Determination of a mean net spectrum for each standard star from the 1985 observations (in units of Flux Number/sec).
- Determination of the 1985 ISC from the 1985 spectra of the standard stars and their relative fluxes.

For each of the standard stars, an ISC was computed from the average 1985 spectra and the absolute fluxes of the standard stars derived as explained above. Average ISC were derived from the OAO and

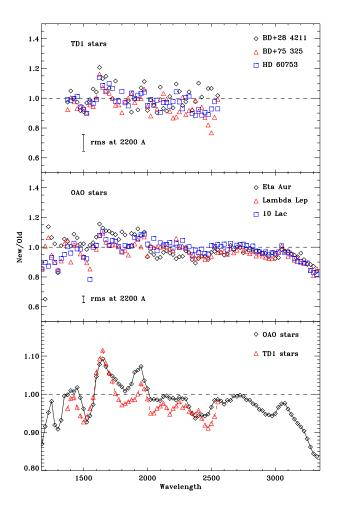


Fig. 1. Comparison of the fluxes of the IUE standard stars derived for the present calibration with those provided by Bohlin and Holm (1984). Shown are the ratios for stars observed with TD1 (upper panel) and with OAO–2 (middle panel). The bottom panel shows the average ratio for the two groups of stars.

TD1 stars. The OAO curve was scaled to the TD1 one, and both were averaged weighting by the number of spectra used in each set. In the case of the LWR camera, separate ISC were derived for both ITFs. The ISCs derived following this procedure are only applicable to low resolution Large Aperture Point spectra. Suitable scaling factors for Small Aperture and Trailed Low Resolution spectra are given by Garhart et al. (1997).

The procedure to derive the high resolution flux calibration from the low resolution calibration is described by Cassatella et al. (2000).

#### 4. Comparison with other calibrations

#### 4.1. Comparison with previous IUE calibrations

As already pointed out in Sec. 2, there was growing evidence that systematic errors were present in the calibra-

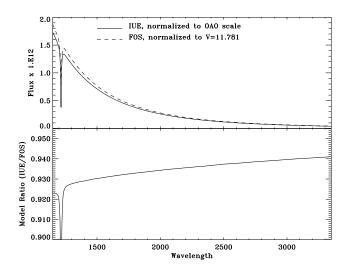


**Fig. 2.** Comparison of the models of the WD G191-B2B used for the calibration of IUE and HST-FOS. The model used for IUE is normalised as to agree with the OAO-2 scale at 2200 Å, i.e. the flux of the model originally normalised to the spectrophotometry of Massey et al. (1988) has been divided by a factor 1.042 (see text).

tions prior to the *IUEFA*. In the following we make a comparison between the present flux calibration and the previous one by ratioing the fluxes of the standard stars used to derive them. The results are shown in Fig. 1, where we represent the ratio between the new and old fluxes for the individual standard stars and, separately, the average ratios for faint (TD1) and bright (OAO-2) standards. To compute these ratios we have used the "corrected" fluxes of the standard stars as given in Bohlin and Holm (1984). We stress that these fluxes are not the original ones provided by the TD1 and OAO-2 experiments, but are corrected using the factors derived by these authors to transfer them into the  $\eta$  UMa scale defined by Bohlin et al. (1980). The discontinuities in the flux ratios shown in the figure clearly indicate the errors in the previous flux scale. These were most likely introduced by the "correction factors" themselves.

In the short wavelength range, there are large fluctuations in the ratios of up to 20% over intervals less than 100 Å wide. The ratio is more uniform between 2000 and 3100 Å and then decreases abruptly, with the new fluxes being lower by up to a 15%. It is interesting to remark that the largest discrepancies are present in the region 1500–1700 Å where, probably not accidentally, the differences between TD1 and OAO–2 fluxes are maximum.

The broad features visible in the flux ratio shown in Fig. 1 are remarkably similar to those of the "correction factor" derived by Finley et al. (1990) from the comparison of atmosphere models and observations of DA white dwarfs, in particular shortward 2000 Å.

## 4.2. Comparison with the HST Absolute Flux Scale

White dwarf models have been used for the flux calibration in the UV range of other space experiments. This is the case of the Hubble Space Telescope and the Hopkins Ultraviolet Telescope (HUT, Kruk et al. 1997, 1999). In the following we will compare the IUE and HST-FOS flux calibrations. The comparison of HUT (both ASTRO–1 and ASTRO–2) and FOS is described in Kruk et al. (1997, 1999).

The absolute calibration of the HST Faint Object Spectrograph is based on a slightly different model of the DA WD G191–B2B (Bohlin et al. 1995) with a pure Hydrogen atmosphere, an effective temperature of 61300 K, log g=7.5, and normalised to V=11.781 (Colina and Bohlin 1994).

The difference in effective temperature of the models used for the calibrations of IUE and FOS results in a slightly different slope in the UV range (approximately 1%, see Fig. 2). The model fluxes used for the IUE calibration (with the original scaling to optical spectrophotometry) are lower than the model used for FOS by 1.1 % at 5500 Å due to the different normalisation. The additional 4.2% scaling factor makes this difference 5.3% at V (in the sense that the FOS model is brighter. This normalisation implies a V magnitude of 11.84 for G191–B2B, in contrast with the recent revision by Bohlin (2000) which derived a value of V=11.773 $\pm$ 0.0012(1  $\sigma$ ).

The slightly different slope of the models increases this discrepancy in the IUE range. The average ratio of the models used in the IUE and the FOS calibrations in the range 1150-3350 Å (excluding the region around Lyman

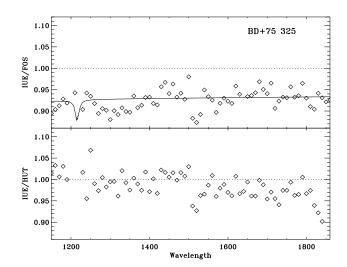


Fig. 3. Comparison of the IUE, HST-FOS and HUT fluxes of the standard star BD+75 325. Shown for comparison in the upper panel is the ratio of the models of the WD G191-2B2 used for the calibration of IUE and FOS (the same as shown at the bottom panel of Fig. 2). This shows that although the relative calibrations are quite consistent, the absolute scale is still rather uncertain.

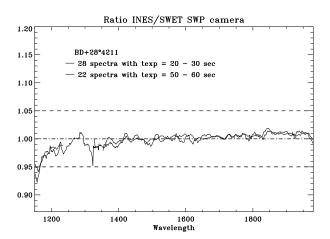


Fig. 4. Average ratio of NEWSIPS and INES fluxes for SWP spectra of the standard star BD+28 4211 (28 spectra with exposure times between 20 and 30 sec. and 22 spectra with exposure times between 50 and 60 sec.). The thin line corresponds to the average ratio for non–saturated spectra, and the thick one to saturated spectra, with only the non–saturated region shown. The dashed lines mark the  $\pm$  5% limits.

 $\alpha)$  is 0.933, i.e. model used for the IUE calibration is lower by a 7.2%.

We have compared the IUE, FOS (Bohlin 1996) and HUT (Kruk, private communication) absolute fluxes of the standard star and BD+75 325 in the spectral region of overlap of the three experiments, as shown in Fig. 3. The continuous line in the upper panel of the figure represents the ratio between the models used for the IUE and FOS calibrations. The average ratios IUE/other over the common wavelength range is  $0.93\pm0.03$  and  $0.99\pm0.05$  for FOS and HUT, respectively. The figure shows that the overall agreement between IUE and FOS flux and model ratios is good, although there are some broad features, which are thought to be induced by the effects of the residual nonlinearities of the IUE cameras on the spectra used for the calibration. On average, the flux ratio IUE/FOS is within a 3% of the model ratio, except for the region 2250-2450 Å where it is lower by a 4%.

The IUE fluxes seem to agree better with the HUT data, but this might simply be an accidental artifact, due to the complex calibration of the different HUT instrumental configurations and the large uncertainties involved (Kruk, private communication).

Although the comparisons in Fig. 3 show a general agreement in the three calibrations (IUE independent of HST and HUT, which are based on the same absolute fluxes), to  $\pm 3\%$  in the relative calibration, it is clear that the absolute UV scale is still uncertain to  $\pm 10\%$ .

## 4.3. Applicability to INES-extracted data

The flux calibration described in this paper has been derived from IUE low resolution spectra processed with

NEWSIPS and the SWET optimal extraction procedure (Garhart et al. 1997). IUE low resolution data have been re-extracted from the NEWSIPS bi-dimensional SILO files using a different algorithm for the INES archive. The INES extraction is described in detail by Rodríguez-Pascual et al. (1999). It includes, among other features, new noise models and an improved extraction procedure. Both extraction algorithms (SWET and INES) use the same inverse sensitivity curve, therefore any differences in the flux calibrated spectra would also appear in NET spectra. Differences of this kind could in principle arise from the different procedures used to estimate the background level, to evaluate the spatial profile, and from the adopted noise model.

In order to check the applicability of the Final Archive calibration to *INES*—extracted data we have taken low resolution spectra of the IUE standard star BD+28 4211 and compared the *INES* and the *NEWSIPS* fluxes. For this purpose we have divided the spectra into two groups according to their level of exposure: the first group containing non–saturated spectra, and the second one containing spectra saturated in the region of maximum sensitivity of the cameras. We have computed the mean ratio for each group of spectra. The results are shown in Fig. 4, Fig. 5 and Fig. 6.

In the SWP camera, the average flux ratio INES/SWET for the short–exposure time spectra is  $1.00\pm0.01$  longward 1250 Å, with a slight slope along the full wavelength range (i.e. the INES flux is slightly lower than the SWET flux shortward 1400 Å and slightly higher longward 1600 Å). Shortward of Lyman  $\alpha$  the INES flux is up to a 8 % lower. The INES flux is also lower in this spectral range for the longest exposure spectra, but only by less than 4%. Longward 1400 Å the flux ratio is  $1.00\pm0.01$  independently on the level of exposure of the spectra.

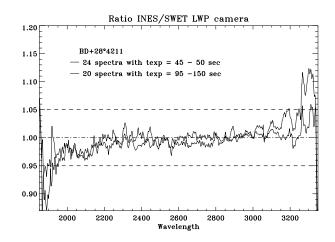


Fig. 5. Same as Fig. 4, but for the LWP camera. Shown are the average ratios corresponding to 24 spectra with exposure times between 45 and 50 sec. and 20 spectra with exposure times between 95 and 150 sec. of the standard star BD+28 4211.

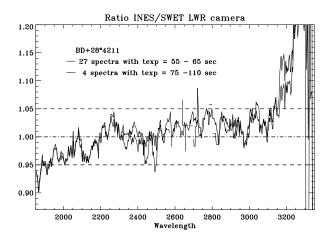


Fig. 6. Same as Fig. 4, but for the LWR camera. Shown are the average ratios for 27 spectra with exposure times between 55 and 65 sec. and 4 spectra with exposure times between 75 and 110 sec. of BD+28 4211. All the spectra have been processed with ITF-B (see Section 3.2) and were taken in the period during which the camera was still operational (1978–1983).

In the case of the LWP camera, the INES and SWET fluxes agree within 1% along most of the spectral range (2200-3000 Å). The largest differences are found at the edges of the range. While at the short wavelengths the INES extraction provides fluxes up to a 10% lower than SWET, the contrary occurs longward 3000 Å where INES fluxes can be a 10% higher. It must be noted that in both cases the differences are larger for short–exposure time spectra, suggesting that the discrepancy can originate from non–linearity effects at low exposure levels.

The largest discrepancies are found in the LWR camera (for images processed with ITF–B). In the region 2500–3000 Å the ratio INES/SWET is  $1.02\pm0.04$ , while at shorter wavelengths (2100–2500 Å) it is closer to unity:  $1.01\pm0.04$ . As in the case of the LWP camera, it is longward 3200 Å where the difference becomes larger, with the INES flux larger by up to a 20%. In this camera there is no significative difference in the behaviour of short and long exposure time spectra.

In summary, the differences between the *INES* and *SWET* extractions are within a 2% over most of the spectra range, with largest differences at the edges of the cameras (in the SWP only at the shortest wavelengths).

#### 5. Conclusions

In this paper we have described the definition of the flux scale which has been adopted for the flux calibration of the IUE Final Archive data. After having discussed the inadequacy of the  $\eta$  UMa flux scale as in Bohlin et al. (1980), we have shown that a more pertinent method which optimizes the internal and external consistency of IUE fluxes is to use the DA white dwarf G191–B2B as primary standard star. The procedure followed consisted basically in using the IUE observations of this star obtained in 1991 together

with model atmosphere fluxes normalized to the data from optical spectrophotometry in Massey et al. (1988) to obtain the shape of the inverse sensitivity curves for the three IUE operational cameras. At this point, the many IUE observations of  $\eta$  Aur,  $\lambda$  Lep, 10 Lac and  $\zeta$  Dra, also obtained in 1991, were used to find a suitable scaling factor of the sensitivity curves such that, after calibration, the scaled fluxes best fitted the corresponding OAO-2 original measurements from Meade (1978) in the range 2100–2300 Å. The choice of this wavelength interval to set the scaling factor was to link the IUE calibration to ultraviolet instead of optical observations. Also, the 2100–2300 Å range is the one where the agreement between TD1 and OAO-2 fluxes is best. As shown in Sect. 3.5, the 2100-2300 Å OAO-2 fluxes of the quoted four standards are on average a factor of 1.042 lower than those from the G191–B2B model normalised to the data from optical spectrophotometry (Massey et al. 1988).

The sensitivity curves for the 1991 epoch, together with the very many observations of the standard stars secured in this epoch were to define the absolute fluxes of the standard stars. These fluxes were then used as input to derive the sensitivity curves for the 1985 calibration epoch (i.e. the epoch the ITFs were obtained for the IUE cameras).

The absolute fluxes of six IUE standard stars and the model fluxes of G191–B2B *in the OAO–2 scale* are given in Appendices A and B, respectively.

As shown in Sec. 4.2, the fluxes obtained with this calibration are on average 7.2% lower than the ones provided by the Faint Object Spectrograph on board the Hubble Space Telescope in the range 1150-3350 Å. This discrepancy can be ascribed to the different choice for scaling the G191–B2B model fluxes and, to a minor extent, to the slightly different stellar parameters adopted for the G191–B2B model.

Rodríguez-Pascual et al. (1999) have discussed the *INES* system and its advantages over *NEWSIPS* to remove the systematic errors found in this latter package. In view of the different extraction software used in the two systems, a specific test has been carried out in this paper to verify the applicability of the present flux scale to low resolution data processed with *INES*. The conclusion is that, in spite of the different extraction algorithms used, the application of the present calibration to *INES* spectra is fully justified. We stress that the present paper has a direct application to the absolute calibration of low resolution spectra. The method used to obtain absolute calibration of high resolution spectra has been discussed elsewhere (Cassatella et al. 2000).

Acknowledgements. We would like to thank the attendees of a Meeting on the IUE flux calibration which we organized at the ESA IUE ground station of Villafranca del Castillo in December 1990, and in particular, Prof. V. Weidemann and Drs. D. Finley, D. Husfeld, D. Koester and D. Massa. We are grateful to Dr. J. Kruk for his comments about the HUT calibration. We would also like to acknowledge the large effort made by the NASA and ESA IUE Observatories in supporting

the calibration activities. This paper is dedicated to the memory of Andy Michalitsianos, who has strongly contributed to the success of the IUE project.

#### References

Barstow, M.A., Fleming, T.A., Finley, D.S., Koester, D., Diamond, C.J., 1993, MNRAS 260, 631

Beeckmans, F., 1977, A&A 60,1

Bohlin, R.C., Holm, A.V., 1984, ESA-IUE Newsletter 20, 22
Bohlin, R.C, Holm, A.V., Savage, B.D., Snijders, M.A.J.,
Sparks, W.M., 1980, A&A 85,1

Bohlin, R.C., Colina, L., Finley, D.S., 1995, AJ 110, 1316

Bohlin, R.C., 1996, AJ 111, 1743.

Bohlin, R.C., 2000, AJ 120, 437.

Bruhweiler, F.C., 1991, Report to the IUE Three Agency Meeting, June 1991

Bruhweiler, F.C., Kondo, Y., 1981, ApJ 248, L123

Brune, W. H., Mount, G. H., Feldman, P. D., 1979, ApJ 227, 884

Cassatella, A., 1990, Report to the IUE Three Agency Meeting, May 1990

Cassatella, A., Altamore, A., González-Riestra, R., et al., 2000, A&AS 141, 331

Colina, L., Bohlin, R.C., 1994, AJ 108, 1931

Finley, D.S., 1993, in "Calibrating HST", ed. J.C. Blades & S.J. Osmer, p. 416

Finley, D. S., Basri, G., Bowyer, S., 1990, ApJ 359, 483

Finley, D.S., Koester, D., Basri, G., 1997, ApJ 488, 375

Garhart, M.P., 1991, Report to the IUE Three Agency Meeting, June 1991, p. VI-38

Garhart, M.P., Smith, M.A., Levay, K.L., Thompsom, R.W., 1997, "International Ultraviolet Explorer New Spectral Image Processing Information Manual, Version 2.0"

González-Riestra, R., 1991, Report to the IUE Three Agency Meeting, June 1991, p. VI-82

González-Riestra, R., 1998, in "Ultraviolet Astrophysics beyond the IUE Final Archive", eds. W. Wamsteker and R. González-Riestra, ESA SP-413, p. 703

González-Riestra, R., Cassatella, A., Solano, E., Altamore, A., Wamsteker, W., 2000, A&AS 141, 343

Greenstein, J. L., Oke, J. B., 1979, ApJ 229, L141

Hackney, R. L., Hackney, K. R. H., Kondo, Y., 1982, in "Advances in Ultraviolet Astronomy", NASA CP-2238, 335

Kimble, R.A., Davidsen, A.F., Blair, W.P., et al., 1993, ApJ 404, 663

Kruk, J.W., Kimble, R.A., Buss, R.H., et al., 1997, ApJ 482, 546

Kruk, J.W., Brown, T. M., Davidsen, A.F., et al., 1999, ApJS 122, 299

Massey, P., Strobel, R., Barnes, J.V., Anderson, E., 1998, ApJ 328, 315

Meade, M., 1978, private communication.

Oliversen, N., 1987, Report to the IUE Three Agency Meeting, November 1987

de la Peña, M., 1992, Report to the IUE Three Agency Meeting, June 1992

Pérez-Calpena, A., Pepoy, J., 1997, "IUE Spacecraft Operations: Final report", ESA SP-1215

Rodríguez-Pascual, P.M., González-Riestra, R., Schartel, N., Wamsteker, W., 1999, A&AS 139, 183

Schartel, N., Skillen, I., 1998, in "Ultraviolet Astrophysics beyond the IUE Final Archive", eds. W. Wamsteker and R. González–Riestra, ESA SP-413, p. 735

Vennes, S., 1992, ApJ 390, 590

Wamsteker, W., 2000, "The INES Newsleter", ESA

Wamsteker, W., Skillen, I., Ponz, J.D., et al., 2000, A&SS, 273, 155

Wolff, B., Koester, D., Dreizler, S., Hass, S., 1998, A&A 329, 1045

# Appendix A: The Absolute Fluxes of the IUE Standard Stars

The tables and figures in Appendix A show the absolute fluxes of the IUE Standard Stars used for the derivation of the cameras Inverse Sensitivity Curves. These fluxes have been derived as described in the text, i.e. the *relative fluxes* with the model of the WD G191 B2B, and the zero point of the scale set by OAO-2 observations. These fluxes define therefore the absolute flux scale of IUE. In all cases the wavelength is in Å and the flux in erg cm $^{-2}$  s $^{-1}$  Å $^{-1}$ . Note that in some cases there are gaps in the data, due to the presence of instrumental artifacts that preclude the accurate determination of the flux in that wavelength bin.

#### Appendix B: The Model Fluxes of G191-B2B

The table in Appendix B gives the model fluxes of the white dwarf G191–B2B from Finley (private communication, 1991). These fluxes are scaled to the OAO–2 flux scale, i.e. the fluxes provided –originally scaled to the optical spectrophotometry of Massey et al. (1988)– have been divided by 1.042. Wavelength is in Å and flux in erg cm<sup>-2</sup> s<sup>-1</sup> Å<sup>-1</sup>.

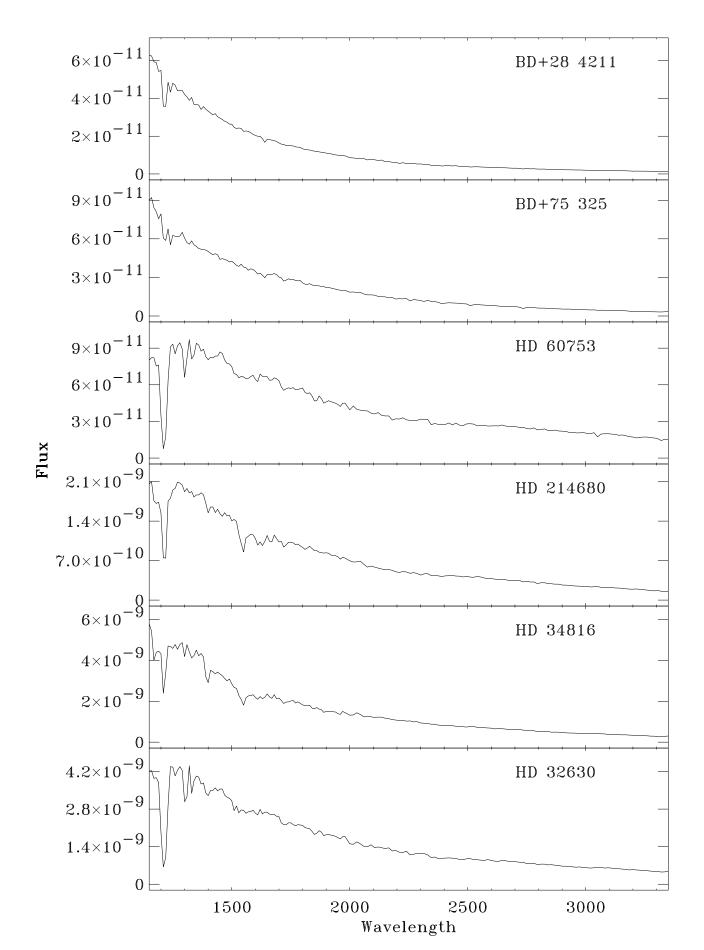


**Table A.1.** BD+28 4211

Wavelength	Flux								
1150	6.27E-11	1500	2.64E-11	1850	1.21E-11	2315	5.03E-12	2840	2.41E-12
1160	6.25E-11	1510	2.47E-11	1860	1.19E-11	2330	5.13E-12	2855	2.45E-12
1170	5.95E-11	1520	2.41E-11	1870	1.17E-11	2345	4.55E-12	2870	2.34E-12
1180	5.90E-11	1530	2.44E-11	1880	1.15E-11	2360	4.53E-12	2885	2.37E-12
1190	5.43E-11	1540	2.41E-11	1890	1.13E-11	2375	4.61E-12	2900	2.27E-12
1200	5.48E-11	1550	2.26E-11	1900	1.10E-11	2390	4.18E-12	2915	2.20E-12
1210	3.59E-11	1560	2.28E-11	1910	1.09E-11	2405	4.37E-12	2930	2.20E-12
1220	3.59E-11	1570	2.26E-11	1920		2420	4.38E-12	2945	2.14E-12
1230	4.86E-11	1580	2.18E-11	1930		2435	4.25E-12	2960	2.10E-12
1240	4.33E-11	1590	2.10E-11	1940	1.01E-11	2450	4.35E-12	2975	2.10E-12
1250	4.80E-11	1600	2.04E-11	1950	9.94E-12	2465	4.06E-12	2990	2.02E-12
1260	4.70E-11	1610	1.00E-11	1960	9.82E-12	2480	3.93E-12	3005	2.00E-12
1270	4.41E-11	1620	1.99E-11	1970	9.67E-12	2495	3.98E-12	3020	1.95E-12
1280	4.41E-11	1630	1.87E-11	1980	9.62E-12	2510	3.68E-12	3035	1.97E-12
1290	4.43E-11	1640	1.68E-11	2000	8.60E-12	2525	3.78E-12	3050	1.68E-12
1300	4.21E-11	1650	1.83E-11	2015	8.48E-12	2540	3.80E-12	3065	1.88E-12
1310	4.09E-11	1660	1.82E-11	2030	8.23E-12	2555	3.68E-12	3080	1.83E-12
1320	3.90E-11	1670	1.79E-11	2045	8.23E-12	2570	3.62E-12	3095	1.83E-12
1330	4.05E-11	1680	1.77E-11	2060	8.10E-12	2585	3.55E-12	3110	1.80E-12
1340	3.68E-11	1690	1.71E-11	2075	7.44E-12	2600	3.55E-12	3125	1.77E-12
1350	3.68E-11	1700	1.64E-11	2090	7.82E-12	2615	3.50E-12	3140	1.68E-12
1360	3.65E-11	1710	1.58E-11	2105	7.50E-12	2630	3.30E-12	3155	1.72E-12
1370	3.42E-11	1720	1.57E-11	2120	7.19E-12	2645	3.28E-12	3170	1.66E-12
1380	3.57E-11	1730	1.50E-11	2135	7.36E-12	2660	3.25E-12	3185	1.60E-12
1390	3.43E-11	1740	1.52E-11	2150	6.51E-12	2675	3.14E-12	3200	1.47E-12
1400	3.33E-11	1750	1.50E-11	2165	6.51E-12	2690	3.04E-12	3215	1.52E-12
1410	3.23E-11	1760	1.49E-11	2180	6.20E-12	2705	3.08E-12	3230	1.49E-12
1420	3.13E-11	1770	1.43E-11	2195	6.19E-12	2720	2.89E-12	3245	1.49E-12
1430	3.20E-11	1780	1.42E-11	2210	5.55E-12	2735	2.64E-12	3260	1.46E-12
1440	3.03E-11	1790	1.41E-11	2225	5.96E-12	2750	2.89E-12	3275	1.44E-12
1450	2.96E-11	1800	1.34E-11	2240	5.50E-12	2765	2.70E-12	3290	1.35E-12
1460	2.89E-11	1810	1.30E-11	2255	5.60E-12	2780	2.74E-12	3305	1.39E-12
1470	2.78E-11	1820	1.28E-11	2270	5.69E-12	2795	2.61E-12	3320	1.35E-12
1480	2.74E-11	1830	1.27E-11	2285	5.26E-12	2810	2.58E-12	3335	1.37E-12
1490	2.64E-11	1840	1.23E-11	2300	5.33E-12	2825	2.60E-12	3350	1.41E-12

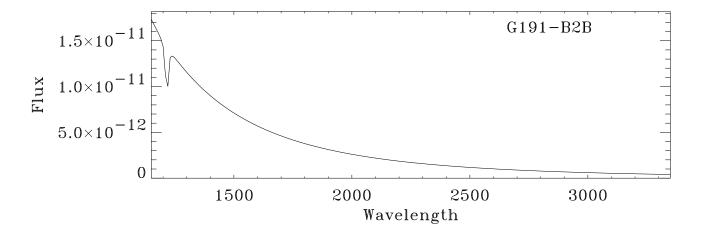


Fig. B.1. UV spectral distribution of the White Dwarf G191–B2B

**Table A.2.** BD+75

Wavelength	Flux								
1150	9.01E-11	1500	4.26E-11	1850	2.36E-11	2315	1.13E-11	2840	5.95E-12
1160	9.20E-11	1510	4.11E-11	1860	2.36E-11	2330	1.22E-11	2855	5.86E-12
1170	8.43E-11	1520	3.93E-11	1870	2.34E-11	2345	1.13E-11	2870	5.60E-12
1180	8.11E-11	1530	3.86E-11	1880	2.29E-11	2360	1.12E-11	2885	5.57E-12
1190	7.56E-11	1540	4.03E-11	1890	2.28E-11	2375	1.07E-11	2900	5.39E-12
1200	7.94E-11	1550	3.80E-11	1900	2.22E-11	2390	9.49E-12	2915	5.38E-12
1210	6.06E-11	1560	3.76E-11	1910	2.22E-11	2405	1.00E-11	2930	5.39E-12
1220	5.88E-11	1570	3.56E-11	1920		2420	1.03E-11	2945	5.15E-12
1230	6.76E-11	1580	3.67E-11	1930		2435	1.01E-11	2960	5.00E-12
1240	5.54E-11	1590	3.62E-11	1940	2.09E-11	2450	1.00E-11	2975	5.05E-12
1250	6.27E-11	1600	3.48E-11	1950	2.06E-11	2465	9.82E-12	2990	4.91E-12
1260	6.20E-11	1610	3.27E-11	1960	2.00E-11	2480	9.49E-12	3005	4.81E-12
1270	6.17E-11	1620	3.34E-11	1970	1.99E-11	2495	9.40E-12	3020	4.69E-12
1280	6.22E-11	1630	3.17E-11	1980	1.99E-11	2510	8.02E-12	3035	4.76E-12
1290	6.50E-11	1640	2.98E-11	2000	1.85E-11	2525	8.72E-12	3050	4.47E-12
1300	6.06E-11	1650	3.22E-11	2015	1.87E-11	2540	9.08E-12	3065	4.53E-12
1310	5.71E-11	1660	3.22E-11	2030	1.81E-11	2555	8.64E-12	3080	4.38E-12
1320	5.58E-11	1670	3.23E-11	2045	1.83E-11	2570	8.49E-12	3095	4.38E-12
1330	5.84E-11	1680	3.31E-11	2060	1.71E-11	2585	8.26E-12	3110	4.36E-12
1340	5.53E-11	1690	3.21E-11	2075	1.64E-11	2600	8.11E-12	3125	4.24E-12
1350	5.41E-11	1700	3.03E-11	2090	1.64E-11	2615	8.07E-12	3140	4.11E-12
1360	5.24E-11	1710	2.96E-11	2105	1.62E-11	2630	7.73E-12	3155	4.10E-12
1370	5.20E-11	1720	2.72E-11	2120	1.53E-11	2645	7.55E-12	3170	4.03E-12
1380	5.16E-11	1730	2.78E-11	2135	1.50E-11	2660	7.47E-12	3185	3.78E-12
1390	5.12E-11	1740	2.89E-11	2150	1.50E-11	2675	7.45E-12	3200	3.26E-12
1400	5.02E-11	1750	2.81E-11	2165	1.41E-11	2690	7.21E-12	3215	3.57E-12
1410	4.88E-11	1760	2.85E-11	2180	1.43E-11	2705	7.25E-12	3230	3.59E-12
1420	4.77E-11	1770	2.76E-11	2195	1.32E-11	2720	6.80E-12	3245	3.63E-12
1430	4.84E-11	1780	2.75E-11	2210	1.34E-11	2735	5.76E-12	3260	3.51E-12
1440	4.77E-11	1790	2.76E-11	2225	1.33E-11	2750	6.72E-12	3275	3.29E-12
1450	4.41E-11	1800	2.58E-11	2240	1.37E-11	2765	6.54E-12	3290	3.27E-12
1460	4.46E-11	1810	2.48E-11	2255	1.17E-11	2780	6.51E-12	3305	3.17E-12
1470	4.40E-11	1820	2.45E-11	2270	1.28E-11	2795	6.19E-12	3320	3.14E-12
1480	4.33E-11	1830	2.52E-11	2285	1.25E-11	2810	6.13E-12	3335	3.27E-12
1490	4.20E-11	1840	2.41E-11	2300	1.20E-11	2825	6.14E-12	3350	3.61E-12

Table A.3.  $\mbox{HD}\ 60753$ 

Wavelength	Flux								
1150	8.01E-11	1500	7.49E-11	1850	4.69E-11	2315	3.15E-11	2840	2.25E-11
1160	8.22E-11	1510	6.91E-11	1860	4.69E-11	2330	3.17E-11	2855	2.24E-11
1170	8.21E-11	1520	6.86E-11	1870	5.09E-11	2345	2.74E-11	2870	2.29E-11
1180	7.54E-11	1530	6.58E-11	1880	4.87E-11	2360	2.83E-11	2885	2.22E-11
1190	7.61E-11	1540	6.68E-11	1890	4.50E-11	2375	2.76E-11	2900	2.20E-11
1200	3.47E-11	1550	6.65E-11	1900	4.60E-11	2390	2.77E-11	2915	2.19E-11
1210	7.63E-12	1560	6.49E-11	1910	4.69E-11	2405	2.75E-11	2930	2.10E-11
1220	1.74E-11	1570	6.53E-11	1920		2420	2.87E-11	2945	2.10E-11
1230	6.33E-11	1580	6.67E-11	1930		2435	2.71E-11	2960	2.06E-11
1240	9.12E-11	1590	6.78E-11	1940	4.49E-11	2450	2.86E-11	2975	2.06E-11
1250	9.32E-11	1600	6.45E-11	1950	4.39E-11	2465	2.70E-11	2990	2.09E-11
1260	8.54E-11	1610	6.26E-11	1960	4.23E-11	2480	2.66E-11	3005	2.02E-11
1270	9.19E-11	1620	6.87E-11	1970	4.49E-11	2495	2.80E-11	3020	2.00E-11
1280	9.44E-11	1630	6.69E-11	1980	4.51E-11	2510	2.81E-11	3035	2.08E-11
1290	8.93E-11	1640	6.69E-11	2000	3.95E-11	2525	2.78E-11	3050	1.74E-11
1300	6.62E-11	1650	6.66E-11	2015	4.26E-11	2540	2.64E-11	3065	1.97E-11
1310	8.16E-11	1660	6.37E-11	2030	3.98E-11	2555	2.65E-11	3080	1.98E-11
1320	9.69E-11	1670	6.39E-11	2045	3.92E-11	2570	2.69E-11	3095	1.99E-11
1330	8.11E-11	1680	6.57E-11	2060	3.87E-11	2585	2.62E-11	3110	1.96E-11
1340	8.44E-11	1690	6.48E-11	2075	3.86E-11	2600	2.63E-11	3125	1.95E-11
1350	9.39E-11	1700	6.33E-11	2090	3.68E-11	2615	2.64E-11	3140	1.86E-11
1360	9.25E-11	1710	5.83E-11	2105	3.61E-11	2630	2.63E-11	3155	1.89E-11
1370	8.76E-11	1720	5.55E-11	2120	3.72E-11	2645	2.71E-11	3170	1.83E-11
1380	8.91E-11	1730	5.67E-11	2135	3.50E-11	2660	2.62E-11	3185	1.75E-11
1390	8.30E-11	1740	5.75E-11	2150	3.45E-11	2675	2.60E-11	3200	1.72E-11
1400	8.05E-11	1750	5.70E-11	2165	3.45E-11	2690	2.56E-11	3215	1.65E-11
1410	8.26E-11	1760	5.77E-11	2180	3.12E-11	2705	2.57E-11	3230	1.70E-11
1420	8.20E-11	1770	5.60E-11	2195	3.21E-11	2720	2.51E-11	3245	1.72E-11
1430	8.36E-11	1780	5.62E-11	2210	3.20E-11	2735	2.52E-11	3260	1.72E-11
1440	8.35E-11	1790		2225	3.30E-11	2750	2.42E-11	3275	1.67E-11
1450	8.69E-11	1800	5.73E-11	2240	3.13E-11	2765	2.38E-11	3290	1.65E-11
1460	8.57E-11	1810	5.39E-11	2255	3.09E-11	2780	2.47E-11	3305	1.59E-11
1470	8.03E-11	1820	5.28E-11	2270	3.10E-11	2795	2.31E-11	3320	1.43E-11
1480	7.74E-11	1830	5.34E-11	2285	3.08E-11	2810	2.33E-11	3335	1.55E-11
1490	7.70E-11	1840	5.10E-11	2300	3.19E-11	2825	2.39E-11	3350	1.51E-11

Table A.4.  $\operatorname{HD}$  32630

Wavelength	Flux								
1150	4.22E-09	1500	3.11E-09	1850	1.86E-09	2315	1.14E-09	2840	7.20E-10
1160	4.23E-09	1510	2.74E-09	1860	1.90E-09	2330	1.09E-09	2855	7.27E-10
1170	3.95E-09	1520	2.91E-09	1870	1.99E-09	2345	9.91E-10	2870	7.09E-10
1180	3.97E-09	1530	2.66E-09	1880	1.94E-09	2360	1.01E-09	2885	6.95E-10
1190	3.79E-09	1540	2.77E-09	1890	1.81E-09	2375	9.56E-10	2900	6.74E-10
1200	1.94E-09	1550	2.76E-09	1900	1.85E-09	2390	9.67E-10	2915	6.71E-10
1210	6.41E-10	1560	2.65E-09	1910	1.85E-09	2405	9.72E-10	2930	6.59E-10
1220	1.00E-09	1570	2.70E-09	1920		2420	9.82E-10	2945	6.45E-10
1230	2.94E-09	1580	2.70E-09	1930		2435	9.72E-10	2960	6.35E-10
1240	4.38E-09	1590	2.76E-09	1940	1.79E-09	2450	9.59E-10	2975	6.44E-10
1250	4.37E-09	1600	2.65E-09	1950	1.74E-09	2465	9.22E-10	2990	6.20E-10
1260	4.04E-09	1610	2.59E-09	1960	1.69E-09	2480	9.15E-10	3005	6.12E-10
1270	4.25E-09	1620	2.79E-09	1970	1.77E-09	2495	9.47E-10	3020	6.03E-10
1280	4.38E-09	1630	2.62E-09	1980	1.71E-09	2510	9.58E-10	3035	6.13E-10
1290	4.24E-09	1640	2.68E-09	2000	1.51E-09	2525	9.12E-10	3050	6.25E-10
1300	3.08E-09	1650	2.69E-09	2015	1.49E-09	2540	9.12E-10	3065	6.24E-10
1310	3.25E-09	1660	2.61E-09	2030	1.58E-09	2555	8.98E-10	3080	6.02E-10
1320	4.41E-09	1670	2.60E-09	2045	1.50E-09	2570	8.85E-10	3095	6.13E-10
1330	3.39E-09	1680	2.60E-09	2060	1.41E-09	2585	9.19E-10	3110	5.98E-10
1340	3.85E-09	1690	2.53E-09	2075	1.40E-09	2600	8.85E-10	3125	5.86E-10
1350	4.03E-09	1700	2.51E-09	2090	1.47E-09	2615	8.59E-10	3140	5.76E-10
1360	3.99E-09	1710	2.28E-09	2105	1.36E-09	2630	8.53E-10	3155	5.63E-10
1370	3.74E-09	1720	2.22E-09	2120	1.39E-09	2645	8.84E-10	3170	5.53E-10
1380	3.77E-09	1730	2.22E-09	2135	1.36E-09	2660	8.79E-10	3185	5.30E-10
1390	3.40E-09	1740	2.29E-09	2150	1.33E-09	2675	8.44E-10	3200	5.49E-10
1400	3.30E-09	1750	2.29E-09	2165	1.36E-09	2690	8.55E-10	3215	5.30E-10
1410	3.50E-09	1760	2.23E-09	2180	1.24E-09	2705	8.35E-10	3230	5.24E-10
1420	3.50E-09	1770	2.18E-09	2195	1.26E-09	2720	8.19E-10	3245	5.02E-10
1430	3.59E-09	1780	2.22E-09	2210	1.19E-09	2735	8.16E-10	3260	5.03E-10
1440	3.48E-09	1790		2225	1.18E-09	2750	7.68E-10	3275	4.89E-10
1450	3.55E-09	1800	2.19E-09	2240	1.23E-09	2765	7.68E-10	3290	4.79E-10
1460	3.55E-09	1810	2.11E-09	2255	1.10E-09	2780	7.81E-10	3305	4.76E-10
1470	3.32E-09	1820	2.09E-09	2270	1.12E-09	2795	7.32E-10	3320	4.54E-10
1480	3.23E-09	1830	2.07E-09	2285	1.15E-09	2810	7.49E-10	3335	4.59E-10
1490	3.21E-09	1840	1.97E-09	2300	1.14E-09	2825	7.48E-10	3350	4.84E-10

Table A.5. HD 34816

Wavelength	Flux								
1150	5.79E-09	1500	2.86E-09	1850	1.63E-09	2315	9.27E-10	2840	5.18E-10
1160	5.44E-09	1510	2.68E-09	1860	1.70E-09	2330	9.11E-10	2855	4.89E-10
1170	4.02E-09	1520	2.64E-09	1870	1.62E-09	2345	8.79E-10	2870	4.91E-10
1180	4.39E-09	1530	2.29E-09	1880	1.58E-09	2360	8.81E-10	2885	4.88E-10
1190	4.45E-09	1540	2.08E-09	1890	1.46E-09	2375	8.35E-10	2900	4.67E-10
1200	4.33E-09	1550	1.81E-09	1900	1.50E-09	2390	8.26E-10	2915	4.57E-10
1210	2.39E-09	1560	2.17E-09	1910	1.51E-09	2405	8.18E-10	2930	4.46E-10
1220	3.38E-09	1570	2.26E-09	1920		2420	8.17E-10	2945	4.44E-10
1230	4.71E-09	1580	2.28E-09	1930		2435	8.05E-10	2960	4.41E-10
1240	4.69E-09	1590	2.32E-09	1940	1.47E-09	2450	7.79E-10	2975	4.25E-10
1250	4.59E-09	1600	2.20E-09	1950	1.39E-09	2465	7.81E-10	2990	4.29E-10
1260	4.78E-09	1610	2.10E-09	1960	1.36E-09	2480	7.56E-10	3005	4.24E-10
1270	4.55E-09	1620	2.23E-09	1970	1.51E-09	2495	7.39E-10	3020	4.19E-10
1280	4.78E-09	1630	2.13E-09	1980	1.45E-09	2510	7.68E-10	3035	4.22E-10
1290	4.87E-09	1640	2.19E-09	2000	1.32E-09	2525	7.62E-10	3050	4.31E-10
1300	4.19E-09	1650	2.36E-09	2015	1.33E-09	2540	7.27E-10	3065	4.09E-10
1310	4.77E-09	1660	2.22E-09	2030	1.44E-09	2555	7.09E-10	3080	4.02E-10
1320	4.43E-09	1670	2.14E-09	2045	1.35E-09	2570	7.07E-10	3095	3.81E-10
1330	4.12E-09	1680	2.32E-09	2060	1.24E-09	2585	6.96E-10	3110	3.89E-10
1340	4.24E-09	1690	2.12E-09	2075	1.27E-09	2600	6.87E-10	3125	3.84E-10
1350	4.51E-09	1700	2.15E-09	2090	1.24E-09	2615	6.48E-10	3140	3.64E-10
1360	4.23E-09	1710	2.04E-09	2105	1.21E-09	2630	6.67E-10	3155	3.56E-10
1370	4.34E-09	1720	1.90E-09	2120	1.23E-09	2645	6.58E-10	3170	3.59E-10
1380	4.17E-09	1730	1.96E-09	2135	1.22E-09	2660	6.42E-10	3185	3.46E-10
1390	3.20E-09	1740	1.97E-09	2150	1.17E-09	2675	6.14E-10	3200	3.37E-10
1400	2.91E-09	1750	2.01E-09	2165	1.15E-09	2690	6.18E-10	3215	3.35E-10
1410	3.52E-09	1760	2.05E-09	2180	1.10E-09	2705	6.10E-10	3230	3.24E-10
1420	3.45E-09	1770	1.92E-09	2195	1.08E-09	2720	6.20E-10	3245	3.20E-10
1430	3.34E-09	1780	1.98E-09	2210	1.06E-09	2735	5.88E-10	3260	3.11E-10
1440	3.43E-09	1790		2225	1.07E-09	2750	5.84E-10	3275	2.94E-10
1450	3.33E-09	1800	1.83E-09	2240	1.03E-09	2765	5.67E-10	3290	2.94E-10
1460	3.26E-09	1810	1.78E-09	2255	1.04E-09	2780	5.60E-10	3305	2.66E-10
1470	3.11E-09	1820	1.79E-09	2270	9.92E-10	2795	5.16E-10	3320	2.87E-10
1480	3.00E-09	1830	1.81E-09	2285	1.01E-09	2810	5.33E-10	3335	2.86E-10
1490	3.09E-09	1840	1.67E-09	2300	9.40E-10	2825	5.34E-10	3350	3.02E-10

Table A.6. HD 214680

Wavelength	Flux								
1150	2.06E-09	1500	1.40E-09	1850	8.77E-10	2315	4.65E-10	2840	2.95E-10
1160	2.10E-09	1510	1.43E-09	1860	8.76E-10	2330	4.70E-10	2855	2.90E-10
1170	1.76E-09	1520	1.40E-09	1870	8.50E-10	2345	4.36E-10	2870	2.83E-10
1180	1.71E-09	1530	1.17E-09	1880	8.39E-10	2360	4.39E-10	2885	2.83E-10
1190	1.73E-09	1540	1.00E-09	1890	8.34E-10	2375	4.30E-10	2900	2.68E-10
1200	1.54E-09	1550	8.54E-10	1900	8.38E-10	2390	4.19E-10	2915	2.65E-10
1210	7.50E-10	1560	1.10E-09	1910	8.32E-10	2405	4.29E-10	2930	2.64E-10
1220	7.44E-10	1570	1.13E-09	1920	7.99E-10	2420	4.32E-10	2945	2.54E-10
1230	1.75E-09	1580	1.17E-09	1930		2435	4.35E-10	2960	2.50E-10
1240	1.81E-09	1590	1.16E-09	1940	7.87E-10	2450	4.26E-10	2975	2.48E-10
1250	1.95E-09	1600	1.09E-09	1950	7.66E-10	2465	4.25E-10	2990	2.41E-10
1260	1.98E-09	1610	9.75E-10	1960	7.26E-10	2480	4.10E-10	3005	2.43E-10
1270	2.09E-09	1620	1.03E-09	1970	7.59E-10	2495	4.24E-10	3020	2.33E-10
1280	2.08E-09	1630	9.68E-10	1980	7.45E-10	2510	4.08E-10	3035	2.37E-10
1290	2.04E-09	1640	1.04E-09	2000	6.97E-10	2525	4.05E-10	3050	2.38E-10
1300	1.92E-09	1650	1.15E-09	2015	6.75E-10	2540	4.19E-10	3065	2.28E-10
1310	1.98E-09	1660	1.04E-09	2030	6.79E-10	2555	4.10E-10	3080	2.27E-10
1320	1.90E-09	1670	1.03E-09	2045	6.90E-10	2570	3.91E-10	3095	2.24E-10
1330	1.92E-09	1680	1.15E-09	2060	6.33E-10	2585	3.84E-10	3110	2.22E-10
1340	1.83E-09	1690	1.09E-09	2075	5.85E-10	2600	3.82E-10	3125	2.16E-10
1350	1.86E-09	1700	1.03E-09	2090	6.03E-10	2615	3.72E-10	3140	2.14E-10
1360	1.86E-09	1710	1.04E-09	2105	5.86E-10	2630	3.66E-10	3155	2.09E-10
1370	1.90E-09	1720	9.40E-10	2120	5.68E-10	2645	3.64E-10	3170	2.01E-10
1380	1.87E-09	1730	9.76E-10	2135	5.51E-10	2660	3.62E-10	3185	1.95E-10
1390	1.71E-09	1740	1.03E-09	2150	5.39E-10	2675	3.47E-10	3200	1.94E-10
1400	1.55E-09	1750	1.02E-09	2165	5.42E-10	2690	3.44E-10	3215	1.98E-10
1410	1.65E-09	1760	1.02E-09	2180	5.27E-10	2705	3.51E-10	3230	1.90E-10
1420	1.65E-09	1770	9.82E-10	2195	5.03E-10	2720	3.45E-10	3245	1.85E-10
1430	1.55E-09	1780	9.94E-10	2210	4.90E-10	2735	3.22E-10	3260	1.78E-10
1440	1.61E-09	1790	9.62E-10	2225	5.06E-10	2750	3.36E-10	3275	1.70E-10
1450	1.53E-09	1800	9.36E-10	2240	4.98E-10	2765	3.21E-10	3290	1.64E-10
1460	1.49E-09	1810	8.99E-10	2255	4.75E-10	2780	3.22E-10	3305	1.70E-10
1470	1.55E-09	1820	9.23E-10	2270	4.87E-10	2795	2.93E-10	3320	1.57E-10
1480	1.49E-09	1830	9.54E-10	2285	4.73E-10	2810	3.07E-10	3335	1.51E-10
1490	1.50E-09	1840	9.16E-10	2300	4.43E-10	2825	3.07E-10	3350	1.50E-10

**Table B.1.** Absolute Fluxes of the White Dwarf G191–B2B

Wavelength	Flux								
1150	1.73E-11	1500	7.11E-12	1850	3.43E-12	2315	1.55E-12	2840	7.38E-13
1160	1.68E-11	1510	6.95E-12	1860	3.37E-12	2330	1.51E-12	2855	7.24E-13
1170	1.63E-11	1520	6.80E-12	1870	3.30E-12	2345	1.48E-12	2870	7.11E-13
1180	1.58E-11	1530	6.65E-12	1880	3.24E-12	2360	1.44E-12	2885	6.97E-13
1190	1.53E-11	1540	6.50E-12	1890	3.18E-12	2375	1.41E-12	2900	6.84E-13
1200	1.44E-11	1550	6.36E-12	1900	3.12E-12	2390	1.38E-12	2915	6.71E-13
1210	1.12E-11	1560	6.22E-12	1910	3.07E-12	2405	1.35E-12	2930	6.59E-13
1220	1.00E-11	1570	6.08E-12	1920	3.01E-12	2420	1.32E-12	2945	6.47E-13
1230	1.32E-11	1580	5.95E-12	1930	2.96E-12	2435	1.29E-12	2960	6.35E-13
1240	1.33E-11	1590	5.82E-12	1940	2.90E-12	2450	1.26E-12	2975	6.23E-13
1250	1.31E-11	1600	5.70E-12	1950	2.85E-12	2465	1.23E-12	2990	6.12E-13
1260	1.28E-11	1610	5.57E-12	1960	2.80E-12	2480	1.21E-12	3005	6.01E-13
1270	1.25E-11	1620	5.46E-12	1970	2.75E-12	2495	1.18E-12	3020	5.90E-13
1280	1.22E-11	1630	5.34E-12	1980	2.70E-12	2510	1.16E-12	3035	5.79E-13
1290	1.19E-11	1640	5.23E-12	2000	2.61E-12	2525	1.13E-12	3050	5.69E-13
1300	1.16E-11	1650	5.12E-12	2015	2.54E-12	2540	1.11E-12	3065	5.59E-13
1310	1.13E-11	1660	5.01E-12	2030	2.47E-12	2555	1.08E-12	3080	5.49E-13
1320	1.10E-11	1670	4.91E-12	2045	2.41E-12	2570	1.06E-12	3095	5.39E-13
1330	1.07E-11	1680	4.81E-12	2060	2.35E-12	2585	1.04E-12	3110	5.30E-13
1340	1.04E-11	1690	4.71E-12	2075	2.29E-12	2600	1.02E-12	3125	5.20E-13
1350	1.02E-11	1700	4.61E-12	2090	2.23E-12	2615	9.97E-13	3140	5.11E-13
1360	9.93E-12	1710	4.52E-12	2105	2.17E-12	2630	9.76E-13	3155	5.02E-13
1370	9.69E-12	1720	4.43E-12	2120	2.12E-12	2645	9.56E-13	3170	4.94E-13
1380	9.46E-12	1730	4.34E-12	2135	2.07E-12	2660	9.37E-13	3185	4.85E-13
1390	9.23E-12	1740	4.25E-12	2150	2.01E-12	2675	9.18E-13	3200	4.77E-13
1400	9.01E-12	1750	4.17E-12	2165	1.97E-12	2690	9.00E-13	3215	4.69E-13
1410	8.79E-12	1760	4.09E-12	2180	1.92E-12	2705	8.82E-13	3230	4.61E-13
1420	8.58E-12	1770	4.01E-12	2195	1.87E-12	2720	8.64E-13	3245	4.53E-13
1430	8.38E-12	1780	3.93E-12	2210	1.83E-12	2735	8.47E-13	3260	4.45E-13
1440	8.18E-12	1790	3.85E-12	2225	1.78E-12	2750	8.30E-13	3275	4.38E-13
1450	7.99E-12	1800	3.78E-12	2240	1.74E-12	2765	8.14E-13	3290	4.31E-13
1460	7.81E-12	1810	3.71E-12	2255	1.70E-12	2780	7.98E-13	3305	4.23E-13
1470	7.62E-12	1820	3.63E-12	2270	1.66E-12	2795	7.83E-13	3320	4.16E-13
1480	7.45E-12	1830	3.57E-12	2285	1.62E-12	2810	7.67E-13	3335	4.10E-13
1490	7.28E-12	1840	3.50E-12	2300	1.58E-12	2825	7.53E-13	3350	4.03E-13